PHYSICAL REVIEW B **93**, 155435 (2016)

Temperature-dependent excitonic effects in the optical properties of single-layer MoS_2

Alejandro Molina-Sánchez,[1] Maurizia Palummo,[2,3] Andrea Marini,[4] and Ludger Wirtz[1]

[1]*Physics and Materials Science Research Unit, University of Luxembourg, 162a avenue de la Faïencerie, L-1511 Luxembourg, Luxembourg*

[2]*University of Rome Tor Vergata, Rome, Italy*

[3]*INFN, Laboratori Nazionali di Frascati, Via E. Fermi 40, I-00044 Frascati, Italy*

[4]*Istituto di Struttura della Materia of the National Research Council, Via Salaria Km 29.3, I-00016 Monterotondo Stazione, Italy*

(Received 11 February 2016; revised manuscript received 30 March 2016; published 26 April 2016)

Temperature influences the performance of two-dimensional (2D) materials in optoelectronic devices. Indeed, the optical characterization of these materials is usually realized at room temperature. Nevertheless, most *ab initio* studies are still performed without including any temperature effect. As a consequence, important features are thus overlooked, such as the relative height of the excitonic peaks and their broadening, directly related to the temperature and to the nonradiative exciton relaxation time. We present *ab initio* calculations of the optical response of single-layer MoS_2, a prototype 2D material, as a function of temperature using density functional theory and many-body perturbation theory. We compute the electron-phonon interaction using the full spinorial wave functions, i.e., fully taking into account the effects of spin-orbit interaction. We find that bound excitons (A and B peaks) and resonant excitons (C peak) exhibit different behavior with temperature, displaying different nonradiative linewidths. We conclude that the inhomogeneous broadening of the absorption spectra is mainly due to electron-phonon scattering mechanisms. Our calculations explain the shortcomings of previous (zero-temperature) theoretical spectra and match well with the experimental spectra acquired at room temperature. Moreover, we disentangle the contributions of acoustic and optical phonon modes to the quasiparticles and exciton linewidths. Our model also allows us to identify which phonon modes couple to each exciton state, which is useful for the interpretation of resonant Raman-scattering experiments.

DOI: 10.1103/PhysRevB.93.155435

I. INTRODUCTION

Ultrathin two-dimensional materials such as graphene and MoS_2 are appealing candidates for a new generation of optoelectronic devices [1] such as photoresponsive memories [2], light-emitting and harvesting devices [3], or nanoscale transistors [4]. They are also suitable platforms for carrying out research on fundamental physics phenomena such as the valley Hall effect [5], ultrafast charge transfer [6], or valley excitons in two-dimensional materials [7]. Technologically, single-layer MoS_2 is relevant due to a direct optical gap at 1.8 eV and a high electron mobility [8].

The optical response of MoS_2 is dominated by strongly bound excitons [9–11]. The same holds for the other group-VI semiconducting single-layer transition-metal dichalcogenides (TMDs) such as MX_2, with M = Mo or W and X = S, Se, or Te [12,13]. This suggests their possible use in optoelectronic devices working at room temperature. Nevertheless, most of the modern first-principles ground- and excited-state simulations are performed at 0 K and thus omit the role of thermal lattice vibrations on the electronic and optical properties.

In general, temperature has a dominant influence on the electronic and optical properties of semiconductors, determining their application as optoelectronic devices [14]. It is well known that it drives the band-gap renormalization [15] and induces changes in the position and width of the optical peaks [16]. At the same time, the spectra obtained from other techniques such as angle-resolved photoemission spectroscopy (ARPES) [17] are also clearly influenced by the temperature due to the enhanced mixing of electron and phonon states.

The possibility to perform electronic structure calculations based on *ab initio* approaches including the electron-phonon (EP) interaction is thus of paramount importance. Even though many years ago [18] Heine, Allen, and Cardona (HAC) pointed out that the EP coupling can induce corrections of the electronic levels as large as those induced by the electronic correlation, the number of works based on first-principles simulations addressing this problem has been very limited and mainly dedicated to traditional bulk compounds [19]. The inclusion of EP couplings considerably broadens the scope of first-principles electronic-structure calculations beyond the study of temperature effects. It opens the way to the study of many interesting phenomena such as polaron formation in crystals and transport properties [20].

As for MoS_2, theoretical *ab initio* studies including the EP interaction have addressed specific aspects such as phonon-limited mobility [21], thermal conductivity [22], electron cooling [23], or electron transport [24]. Tongay *et al.* [25] have performed a theoretical and experimental study of the band-gap dependence on temperature for multilayer $MoSe_2$ and MoS_2. They have attributed all temperature effects to lattice renormalization induced by the thermal expansion. They capture correctly the band-gap trend only for high temperatures (above 300 K). Below room temperature, the electron-phonon interaction plays a crucial role, but it is ignored by Tongay *et al.* [25]. In Ref. [11], Qiu *et al.* have studied temperature effects by including the quasiparticle linewidths. However, they ignored the energy renormalization and the accurate calculation of the linewidths across all the Brillouin zone. Here we use a fully *ab initio* approach to study how the EP interaction induces changes in the electronic structure and optical properties of the MoS_2 single layer. This also enables us to address photoluminescence [26], ARPES [17,27], and resonant Raman-scattering experiments [28].

Differently from most of the recent works on bulk materials [29], we do not limit our study to the band-gap renormalization but we extend our investigation to the full band structure, with special attention to the electron states of interest for optoelectronic applications. Starting from previous studies which established the existence of several kinds of excitonic states in this low-dimensional material [10,11], whose behavior we characterize as a function of the temperature, we calculate the shift of the binding energy and the nonradiative linewidths of excited states.

It is worthwhile to note that in our approach, we use the full spinorial nature of the wave functions through all ground- and excited-state calculations. This is quite important because it is well known that spin-orbit coupling determines the valley polarization dynamics and is fundamental to understand the optical properties of all TMDs.

II. THE THEORETICAL APPROACH

Our calculations start with density functional theory (DFT) to obtain a first estimate of the electronic bands. We use density functional perturbation theory (DFPT) to calculate the phonon modes and the electron-phonon coupling matrix elements. With the latter, we calculate the change of the electronic bands due to the lattice vibrations [30]. Afterwards, we solve the temperature-dependent Bethe-Salpeter equation [31]. We thus explore the change in the optical spectra, and in the exciton energies and linewidths when temperature increases.

The ground-state properties of single-layer MoS_2, eigenvalues, and wave functions are calculated with the QUANTUM ESPRESSO code [32] within the local-density approximation (LDA) for the exchange-correlation potential. We use DFPT to obtain the phonon modes as well as the first- and second-order electron-phonon matrix elements [33]. As mentioned in Sec. I, the spin-orbit interaction is essential to correctly describe excitons in MoS_2 and, for this reason, the electron-phonon matrix elements are also calculated taking into account the full spinor wave functions.

We study the temperature effects on the electronic states and on the excitons by merging DFT/DFPT with many-body perturbation theory. Within this framework, two self-energy diagrams, which correspond to the lowest nonvanishing terms of a perturbative treatment, have to be evaluated. The Fan self-energy [33], related to first-order terms, is

$$\Sigma^{Fan}_{n,\mathbf{k}}(\omega,T)=\sum_{n'\mathbf{q}\lambda}\frac{\left|g^{\mathbf{q}\lambda}_{nn'\mathbf{k}}\right|^2}{N_q}\left[\frac{N_{\mathbf{q}}(T)+1-f_{n'\mathbf{k}-\mathbf{q}}}{\omega-\varepsilon_{n'\mathbf{k}-\mathbf{q}}-\omega_{\mathbf{q}\lambda}-i0^+}\right]\times\left[\frac{N_{\mathbf{q}}(T)+f_{n'\mathbf{k}-\mathbf{q}}}{\omega-\varepsilon_{n'\mathbf{k}-\mathbf{q}}+\omega_{\mathbf{q}\lambda}-i0^+}\right], \quad (1)$$

where $\varepsilon_{n,\mathbf{k}}$ are the LDA eigenvalues, $\omega_{\mathbf{q},\lambda}$ are the phonon frequencies, and $f_{n,\mathbf{k}}$ and $N_{\mathbf{q}}(T)$ are the Fermi and Bose distribution functions of electrons and phonons, respectively. The self-energy associated to an electron state $(n,\mathbf{k})$ is the sum over all the electron states n' and phonon modes λ, where N_q is the number of $\mathbf{q}$ vectors in the Brillouin zone. Conservation of momentum is explicitly enforced. The first-order electron-phonon matrix elements $g^{\mathbf{q}\lambda}_{nn'\mathbf{k}}$ represent the amplitude for the scattering process $|n\mathbf{k}\rangle\rightarrow|n'\mathbf{k}-\mathbf{q}\rangle\otimes|\mathbf{q}\lambda\rangle$ [30]. We have a similar expression for the Debye-Waller (DW) self-energy, related to the second-order terms,

$$\Sigma^{DW}_{n,\mathbf{k}}(T)=\frac{1}{N_q}\sum_{\mathbf{q}\lambda}\Lambda^{\mathbf{q}\lambda,-\mathbf{q}\lambda}_{nn\mathbf{k}}[2N_{\mathbf{q}\lambda}(T)+1], \quad (2)$$

where instead $\Lambda^{\mathbf{q}\lambda,\mathbf{q}'\lambda'}_{nn'\mathbf{k}}$ represents the amplitude for the second-order scattering process $|n\mathbf{k}\rangle\rightarrow|n',\mathbf{k}-\mathbf{q}-\mathbf{q}'\rangle\otimes|\mathbf{q}\lambda\rangle\otimes|\mathbf{q}'\lambda'\rangle$ [30]. In both self-energy terms, temperature enters via the phonon population. In polar semiconductors, the electron-phonon interaction strength becomes larger when including the Fröhlich polar-coupling term [34]. Nonetheless, the longitudinal optic–transverse optical (LO-TO) splitting in bulk MoS_2 is rather small, i.e., 3 cm^{-1}, and we do not expect significant changes in single layer.

The fully interacting electron propagator (accounting for the electron-phonon interaction) is

$$G_{n\mathbf{k}}(\omega,T)=\left[\omega-\varepsilon_{n\mathbf{k}}-\Sigma^{Fan}_{n\mathbf{k}}(\omega,T)-\Sigma^{DW}_{n\mathbf{k}}(T)\right]^{-1}. \quad (3)$$

The complex poles of this equation define the electronic excitations of the interacting system. If the quasiparticle approximation (QPA) is valid, and assuming a smooth frequency dependence, the electron-phonon self-energy can be expanded up to the first order around the bare energies ($\varepsilon_{n\mathbf{k}}$). In this case, the temperature-dependent quasiparticle energies are defined as [35]

$$E_{n\mathbf{k}}(T)=\varepsilon_{n\mathbf{k}}+Z_{n\mathbf{k}}(T)\left[\Sigma^{Fan}_{n\mathbf{k}}(\varepsilon_{n\mathbf{k}},T)+\Sigma^{DW}_{n\mathbf{k}}(T)\right]. \quad (4)$$

It is clear that the quasiparticle energies depend on temperature and are complex numbers, where the real parts are the quasiparticle energies and the imaginary parts $\Gamma_{n\mathbf{k}}(T)$ correspond to the quasiparticle widths. The renormalization factor $Z_{n\mathbf{k}}$ represents the quasiparticle charge. Therefore, the QPA makes sense when $Z_{n\mathbf{k}}$ takes a value close to 1. If the QPA holds, then the spectral function $A_{n\mathbf{k}}(\omega,T)$, i.e., the imaginary part of the Green's function, is a single-peak Lorentzian function centered at $E_{n\mathbf{k}}$ and with width $\Gamma_{n\mathbf{k}}(T)$. The narrower the spectral function is, the weaker the electron-lattice interaction is. When the electron-lattice interaction becomes strong enough, the QPA breaks down, and the spectral functions no longer consist of Lorentzian peaks but span a wide energy range [33].

III. TEMPERATURE-DEPENDENT ELECTRONIC STRUCTURE OF SINGLE-LAYER MoS_2

The calculation of the electronic structure of MoS_2 has been done in a plane-wave basis using norm-conserving pseudopotentials and a kinetic-energy cutoff of 80 Ry and a $\mathbf{k}$ grid of $12\times12\times1$. On top of self-consistent DFT simulations, electron-phonon matrix elements are obtained by DFPT in the local-density approximation. From the explicit expressions of the self-energy terms [Eqs. (1) and (2)], it becomes clear that a careful convergence over the number of bands n' and the number of transferred phonon momenta $\mathbf{q}$ to evaluate the integral over the Brillouin zone is required. From our study, we have found that the spectral functions of MoS_2 converge using a set of 400 randomly distributed

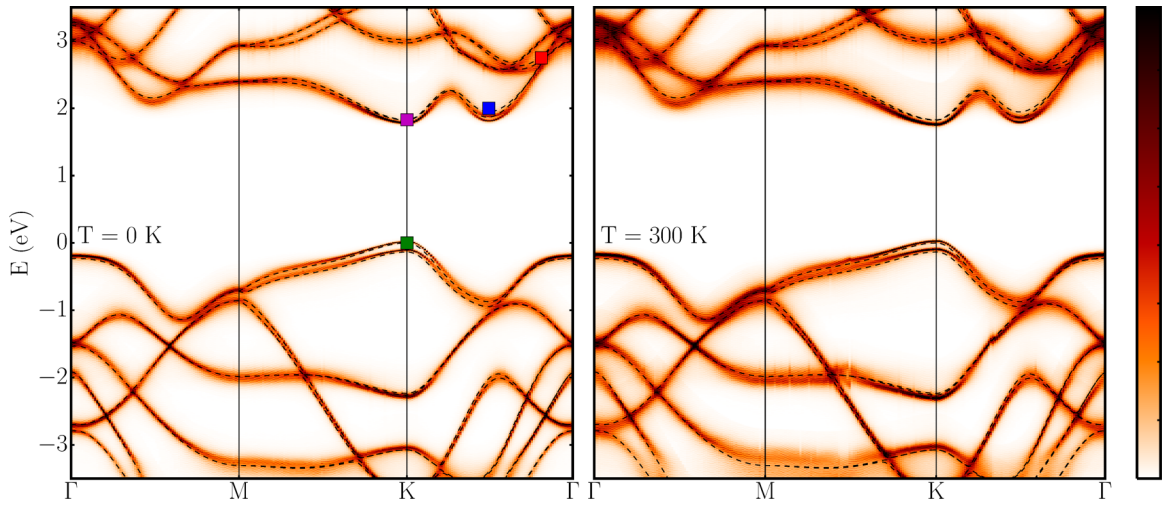

FIG. 1. Spectral functions of single-layer MoS_2 for temperatures 0 K (left panel) and 300 K (right panel). The colored squares denote the points T_c (red), $T_{c'}$ (blue), K_c (purple), and K_v (green). Spectral function is normalized. The color scale bar indicates the maximum value in black and the minimum value in white.

q points and 36 bands (18 occupied bands—we do not take into account Mo-semicore electrons—and 18 empty bands). The calculations are converged with respect to the number of **q** points and bands. We have checked this on the profile of the spectral function, which is a more stringent test than checking the eigenvalue correction. We have used a Lorentzian broadening of 60 meV. Recent works on diamond and silicon required a much larger number of bands and **q** points to reach convergence [36]. The rapid convergence with the number of **q** points we have found here is mainly due to the two-dimensional nature of the material under investigation.

Figure 1 shows the spectral function of single-layer MoS_2 for temperature 0 K (left panel) and 300 K (right panel). An animated representation of the band structures for temperature ranging from 0 to 1000 K in steps of 100 K can be found in the Supplemental Material [37]. Dotted black lines represent the LDA band structure (without electron-phonon interaction). We have marked with squares some important points in the band structures, which will be discussed in more detail below. The bands are no longer a line and they acquire a broadening. This broadening is directly related to the linewidths of each quasiparticle state. Considering that lifetimes are inversely proportional to linewidths, narrow lines are related to long lifetimes, i.e., stable states. In contrast, broader states have a stronger interaction with phonons and they have more nonradiative recombination paths, meaning a shorter lifetime.

We identify very narrow line shapes at the band edges such as the valence-band states at the $\boldsymbol{K}$ and Γ points. In the conduction band, we find narrow line shapes at $\boldsymbol{K}$ and at the minimum between $\boldsymbol{K}$ and Γ. Temperature tends to reduce the quasiparticle energy, but it does not significantly change the spectral function; it only moves the maximum to lower energies. The increase of temperature results in a shrinking of the gap. Even at 0 K, the gap is diminished by 75 meV (with respect to its value calculated without electron-phonon coupling). This is an effect of the zero-point vibrations of the atoms.

The spectral functions of quasiparticle states far from the band edges have a different aspect. Close to crossings, the bands become blurred, making it difficult to distinguish individual bands. For instance, the conduction band around Γ and the crossing close to $\boldsymbol{M}$ have a noticeable broadening, even at 0 K. The M point also shows broader bands than the Γ and the $\boldsymbol{K}$ point. The increasing of temperature further blurs the reminiscence of the LDA band dispersion. In areas close to Γ, the band index becomes almost obsolete and we observe a wide spectral range [38]. It is worthwhile to note that quasiparticle states are not necessarily broadened peaks centered at the renormalized electron energy. They can also be mixed states, which can have a structure that is very different from the superposition of the electron and hole density of states. We also expect important consequences on the optical properties. Excitons from states in this range of energies (such as the resonant or van Hove exciton [10,11]) should be affected by the increase of temperature much more than those coming from band edges.

Figure 2 represents the spectral function of the quasiparticle states that are marked with squares in Fig. 1. We have selected three temperatures, i.e., 0 K (dotted line), 300 K (dashed line) and 1000 K (solid line). The arrow indicates the LDA energy. Even though 1000 K is a very high temperature for common experiments, it can help us conceptually to discuss the nature of the electron-phonon interaction. Figures 2(a) and 2(b) show the conduction- and valence-band extrema at $\boldsymbol{K}$. We observe a shift of the peaks with a slight broadening, but always conserving the Lorentzian shape. For the conduction-band states, the electron-phonon interaction conserves the spin degeneracy. However, the valence-band states are split due to the spin-orbit interaction. Comparison with MoS_2 ARPES data collected at 80 K is a delicate issue [17]. Experimental broadening is not exclusively related to electron-phonon decay. Nevertheless, the measured spin-orbit splitting of 145 meV agrees very well with our calculation of 135 meV.

Figure 2(c) shows the spectral function of the state in the local minimum between $\boldsymbol{K}$ and Γ. This spectral function has

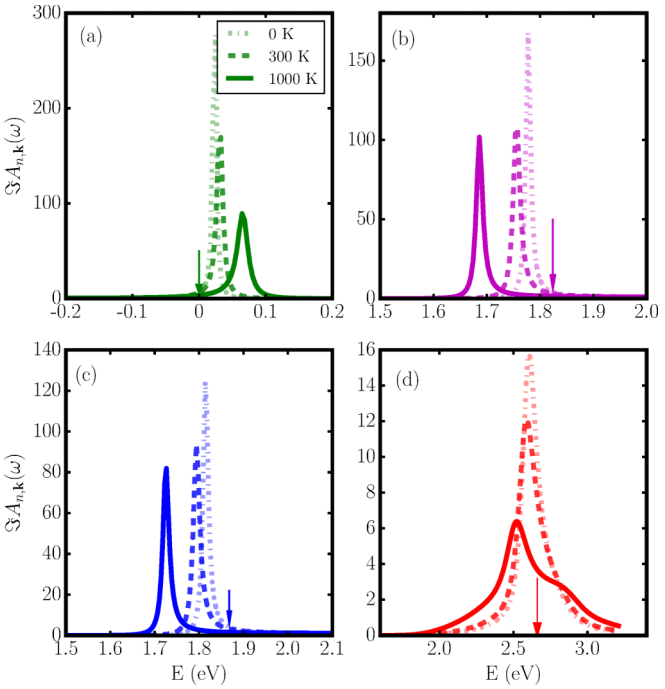

FIG. 2. Spectral functions for selected band states in Fig. 1: T_c (red), T_c' (blue), K_c (magenta), and K_v (green), and for $T = 0$ K (dotted line), 300 K (dashed line), and 1000 K (solid line).

a similar behavior as the cases of Figs. 2(a) and 2(b), but its asymmetry is stronger. This result is compatible with the exposition of Ref. [39], in which transitions are possible from this local minima to the point $\boldsymbol{K}$.

We have found a signature of a potential breakdown of the quasiparticle approximation for some states above the band gap. Figure 2(d) shows a drastic change of the spectral function due to temperature effects. We have chosen a band close to Γ, relevant for describing the exciton C. The shape even at 300 K becomes asymmetric and, when we reach 1000 K, a secondary peak emerges. Notice that the high-energy peak is separated from the low-energy one by an energy far larger than any phonon in MoS_2 [40]. This latter peak appears at higher energy of the LDA energy, contrary to the other spectral functions. This is a proof of the many-body character of the new state and of the breakdown of the quasiparticle approximation. The new states can no longer be interpreted as an independent sum of electrons and phonon replica. The energy separation between the shoulder and the lower peak is bigger than any phonon frequency. Following Ref. [41], the electron is fragmented in several entangled electron-phonon states as a result of virtual transitions not bound to respect the energy conservation. This explains the appearance of these structures in a wide energy range [33].

We follow the analysis of the temperature-dependent electronic structure by investigating the band-gap renormalization. We have seen that at 0 K, the band gap of single-layer MoS_2 shrinks. The reason is the uncertainty principle and this is known as the zero-point motion renormalization (ZPR) effect. At 0 K, atoms cannot be at rest and have zero velocity; there is a minimum quantum of energy which supplies the vibration which makes possible the electron-phonon interaction. Table I

TABLE I. Zero-point motion renormalization of single-layer MoS_2, diamond, SiC, and Si.

	ZPR (meV)
MoS_2	75
Diamond	622 [29]
SiC	223 [42]
Si	123 [42]

shows the ZPR for several semiconductors, calculated in previous works. Single-layer MoS_2 exhibits a smaller ZPR effect, especially in comparison with diamond. The wave function of the conduction- and valence-band state at $\boldsymbol{K}$ is mostly concentrated around the molybdenum atoms. The large mass of molybdenum reduces the phonon amplitude, with the consequence of a smaller correction.

In order to shed light on which phonon modes contribute to the electron-phonon interaction, it is useful to calculate the Eliashberg functions,

$$g^2 F_{n\mathbf{k}}(\omega) = \sum_{\lambda\mathbf{q}} \left[\frac{\sum_{n'} |g^{\mathbf{q}\lambda}_{nn'\mathbf{k}}|^2 N_{\mathbf{q}}^{-1}}{\varepsilon_{n\mathbf{k}} - \varepsilon_{n'\mathbf{k}+\mathbf{q}}} \right] \delta(\omega - \omega_{\mathbf{q}\lambda}) - \sum_{\lambda\mathbf{q}} \left[2 \frac{\sum_{n'} \Lambda^{\mathbf{q}\lambda}_{nn'\mathbf{k}} N_{\mathbf{q}}^{-1}}{\varepsilon_{n\mathbf{k}} - \varepsilon_{n'\mathbf{k}}} \right] \delta(\omega - \omega_{\mathbf{q}\lambda}). \quad (5)$$

Figure 3 shows the phonon dispersion of single-layer MoS_2 [Fig. 3(a)], together with the phonon density of states [Fig. 3(b)] and the Eliashberg functions [Figs. 3(c)–3(e)], calculated for the quasiparticle states marked with the same color in Figs. 1 and 2. In Fig. 3(a), the color of the phonon-dispersion curves indicates the vibration-mode direction: vibrations in-plane are represented by red dots and out-of-plane vibrations are represented by blue dots.

A common trend of all the Eliashberg functions is the absence of acoustic-phonon contributions close to Γ. In calculations without the DW term (not shown here), there is a finite contribution of the Fan-Eliashberg function, which is removed once the DW is added. Therefore, even though the DW term has a small contribution, it is important in order to achieve accurate results. The states at K [Fig. 3(d)] have similar Eliashberg functions, which are almost symmetric. They have opposite sign, which results in the shrinking of the band gap. The main contributions come from phonons at the edge of the Brillouin zone around 200 cm^{-1} and from optical phonons around 400 cm^{-1}. In the case of the phonons of the state T_c [Fig. 3(e)], we find a similar Eliashberg function. The high-frequency contribution is almost identical to the one of the state K_c.

The Eliashberg function for the state close to Γ [Fig. 3(c)] has a different shape than the others. There is no contribution from midfrequency phonons. The main interaction is due to optical phonons, around 380 cm^{-1}. In this case, the Eliashberg function changes the sign, crossing the zero axis several times (dotted lines). The Eliashberg functions shown in Fig. 3(d) are centered close to the frequency of mode A_{1g},

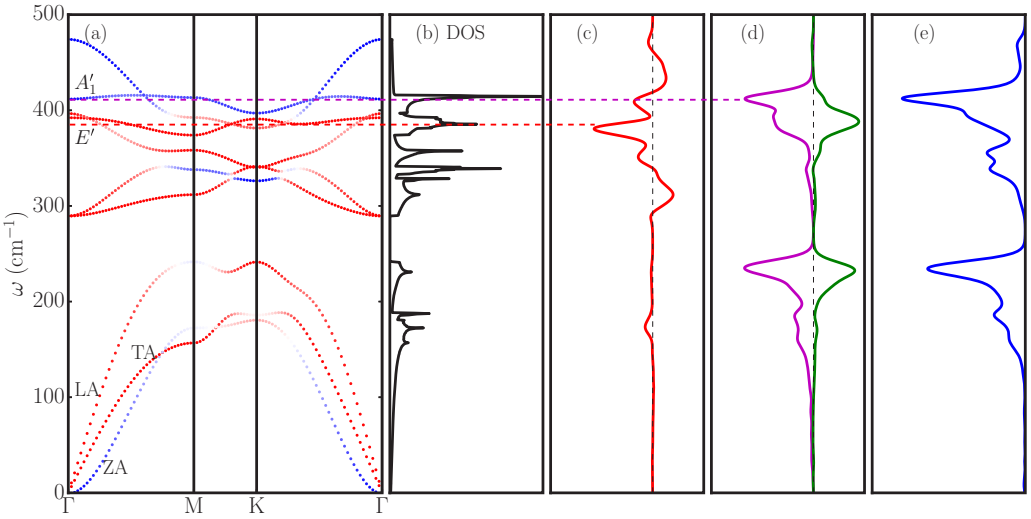

FIG. 3. Phonon band structure and density of states of single-layer MoS_2. Eliashberg functions of the band states T_c, T_c', K_c, and K_v (see definitions in the text).

in a frequency range exclusively populated by out-of-plane phonons. In contrast, the function in Fig. 3(c) is built from in-plane phonons close to the frequency of the phonon mode E_{2g}. These findings seem to support the conclusion reached in a recent work by Carvalho *et al.* [28] on the basis of pure symmetry arguments. Measuring Raman spectra of a MoS_2 monolayer, they concluded that exciton A couples with phonon mode A_{1g}, while exciton C couples with phonon mode E_{2g} [10,11].

Since excitons and phonons are particularly complex in TMDs, some deviations can occur as excitons are built from many electron and hole states of different electron momentum **k** and we are just examining a few states. We have analyzed the Eliashberg functions at different k points (around K and Γ), observing a small energy shift but no drastic changes under small changes of **k**. From this result, we can affirm that the identification of Ref. [28] corresponds to the excitons A and C. A definitive proof of this statement would consist of calculating the Raman tensor [43] (in resonant conditions), but this is beyond the scope of our work.

IV. FINITE-TEMPERATURE EXCITONIC EFFECTS ON THE OPTICAL ABSORPTION

As mentioned in Sec. I, it is well known that temperature not only affects the energies but also the widths of the peaks in the optical spectra of materials. Here, we systematically study the behavior of the absorption spectrum of MoS_2 (both as single layer and bulk) on temperature. Previously, only the low-energy A exciton has been measured in photoluminescence at different temperature [44]. Measurements of the absorption (reflectance) spectra of MoS_2 are usually done at room temperature.

From the theoretical point of view, if electron-phonon interaction is not taken into account, then the *ab initio* optical spectra are restricted to the use of a homogeneous *ad hoc* broadening. Here, following Ref. [31], we solve the temperature-dependent Bethe-Salpeter equation, where the corresponding excitonic Hamiltonian is

$$H^{FA}_{ee'hh'} = [E_e + \Delta E_e(T) - E_h - \Delta E_h(T)]\delta_{eh,e'h'} + (f_e - f_h)\Xi_{ee'hh'}, \quad (6)$$

in which E_e and E_h stand for electron and hole energies, respectively, f_e and f_h are the occupations, and $\Xi_{ee'hh'}$ is the Bethe-Salpeter (BS) kernel [31,45]. $\Delta E_e(T)$ and $\Delta E_h(T)$ stand for the renormalization of the electron and hole energies through the EP interaction, as calculated in Eq. (4). The BS kernel is the sum of the direct and exchange electron-hole scattering. In a temperature-independent formulation, we would calculate the energies and the BS kernel from DFT with the corresponding GW corrections to take care of the band-gap underestimation inherent to DFT [46]. In this work, we have used a scissor operator of 0.925 eV and a stretching factor of 1.2 for the conduction and valence bands. These values were obtained by comparison of the DFT-LDA band structure with a GW calculation for single-layer MoS_2 [13,47]. In the temperature-dependent approach, we use the QP eigenvalues obtained from Eq. (4), which now are complex numbers and depend on temperature. As said above, the finite linewidth is given as the imaginary part of the eigenvalue correction. The temperature-dependent BS equation (6) contains a non-Hermitian operator. The excitonic states will thus have a complex energy $E^X(T)$ depending on temperature and the imaginary part represents the nonradiative linewidth of the exciton [31]. Moreover, temperature not only changes the energy of the excitonic states, but also adds the imaginary term for the linewidth. In systems with a strong electron-lattice interaction, temperature-dependent excitonic states are a mixture of the excitonic states from the temperature-independent regime. For instance, in hexagonal boron nitride, temperature dramatically changes the oscillator strength of the excitons and one observes a temperature-driven transition from dark to bright exciton [31]. Certainly, the temperature effect will also depend on the kind of excitons, as we will see below. It is also worthwhile to mention that at $T = 0$ K the BS equation does not reduce to the frozen-atom

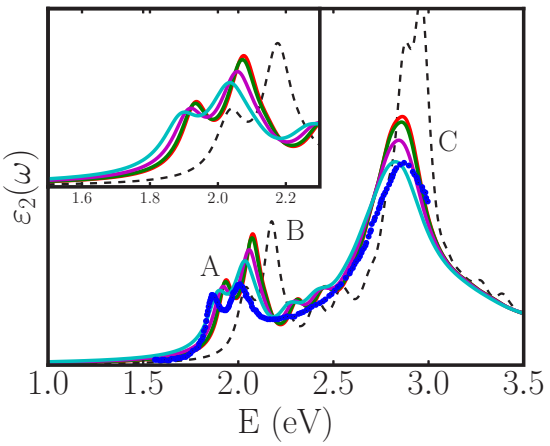

FIG. 4. Optical spectra of single-layer MoS_2 as a function of temperature. The dashed line represents optical spectra without temperature effects, and the solid lines represent spectra at increasing temperature: 0, 100, 200, and 300 K (red, green, magenta, cyan). Dots are experimental data from Ref. [26].

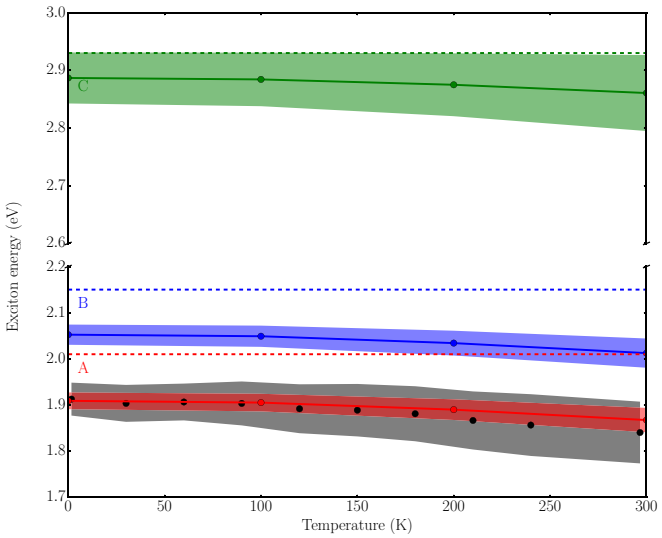

FIG. 5. Exciton energy as a function of temperature (solid lines). The shadow region shows the width of each exciton. The dashed line marks the exciton energy without electron-phonon interaction. The photoluminescence data of Ref. [44] are represented by black dots and the FWHM by the gray area.

approximation due to zero-point vibrations. We only recover the BS equation within the frozen-atom approximation when the terms $\Delta E_e(T)$ and $\Delta E_h(T)$ are explicitly removed.

The dielectric function [31] depends explicitly on the temperature

$$\varepsilon(\omega,T) \propto \sum_X |S_X(T)|^2 \mathrm{Im}\left[\frac{1}{\omega - E_X(T)}\right], \qquad (7)$$

where $S_X(T)$ is the oscillator strength of each exciton. The broadening of the excitonic peaks is introduced naturally as the imaginary part of the exciton energy, without introducing any damping parameter. It is worthwhile to notice than the linewidth associated with the electron-electron interaction is negligible in the energy range in which we study the optical spectra.

Figure 4 shows the Bethe-Salpeter spectra calculated without electron-phonon interaction (black dashed line) and with electron-phonon interaction at 0, 100, 200, and 300 K (red, green, magenta, and cyan, respectively), and the experimental data (dots) at room temperature from Ref. [26]. The change on the electronic states due to temperature has a repercussion on the excitons and on the optical spectra. We have calculated the Bethe-Salpeter spectra in a $30 \times 30 \times 1$ **k** grid, for four conduction-band states and two valence-band states. The rest of the convergence criteria can be found elsewhere [10]. The temperature correction to the quasiparticle states has been done in the same **k** grid and following the previous convergence criteria with respect to the number of bands and **q** points.

The *A* and *B* excitons are shifted down in energy, but the intensity is rather constant. The *A* peak is slightly narrower than the *B* peak, in agreement with the experiments. The *B* excitons are build mainly from the second valence-band maximum, which has more nonradiative paths for recombination than the *A* exciton. The behavior of the *C* exciton is drastically different from that of the *A* and *B* excitons. The *C* exciton comes from transitions close to Γ. In this region of the band structure, the electron-phonon interaction substantially alters the width of the electronic states but not the energy. The intensity drops remarkably from the BS spectrum in the absence of electron-phonon interaction. It is worthwhile to notice that we have used a homogeneous broadening of 50 meV for the BS spectra without electron-phonon interaction. The increasing of temperature reduces the height of the *C*-exciton peak with a faster pace than in the case of the others excitons and also increases the width. Another effect is the collapse of the multipeak structure at the LDA spectra in one broad peak. The result is consistent with the spectral functions of Figs. 1 and 2.

In order to see in a clearer way the temperature effects on the exciton energies, Fig. 5 shows the exciton energy as a function of temperature. The dashed area stands for the width of every excitonic state. The dashed line represents the exciton energy without electron-phonon interaction. All of the excitonic states decrease their energy with increasing temperature, but not at the same pace. The biggest correction to the energy of the excitons *A* and *B* is made by the ZPR, being very similar to both states (100 meV). We can see that the width of these states is almost constant with the increase of temperature, being only slightly bigger for the *B* exciton (44 vs 36 meV). In the case of the *C* excitons, we have a surprising behavior. We expected a larger ZPR correction, proportional to the width. While the width is already large (88 meV at 0 K and 132 meV at 300 K), the temperature increase does not imply a strong correction of the excitonic energy, which remains rather constant. From the spectral functions of Figs. 1 and 2(d), we can see that the states close to Γ exhibit a remarkable increase of the broadening, but it seems to be more or less centered at the same energy. We have added the photoluminescence results of Ref. [44], representing the full width at half maximum (FWHM), with the gray dashed area. The energies show a good agreement at low temperatures and diverge slightly starting at 200 K. The main cause of this disagreement is the thermal expansion, not included in our calculations. Regarding the widths, both experimental and theoretical values increase with temperature,

but the experimental values do so to a larger extent. This suggests that the contribution of more processes such as the radiative recombination have larger lifetimes than the carrier-phonon scattering processes described here. From the theoretical results, we can infer that the band-gap dependence on temperature is dictated mainly by EP interaction, whereas linewidths are influenced by other processes such as radiative recombination or defect scattering [44].

The comparison with the experimental data is rather satisfactory. We can explain the broadening of the *C* peak as the coupling of the electron with lattice vibrations. On the other side, the *A* and *B* peaks also compare well. The approximation made for modeling the *C* exciton seems to be valid, at least to give a qualitative explanation of the spectral width. It is worthwhile to note that modeling temperature effects on the optical properties cannot rely only on the thermal expansion [25], especially at temperatures below 200 K where the thermal expansion is small. Only by taking into account the electron-phonon interaction can we calculate nonradiative linewidths and interpret some data from photoluminescence spectra, such as the FWHM or the broadening of the optical spectra.

V. CONCLUSIONS

We have presented calculations of temperature effects on the electronic structure and the optical properties of a two-dimensional (2D) material in the presence of spin-orbit coupling. For this purpose, we have calculated the electron-phonon matrix elements and the temperature-dependent spectral function using full spinorial wave functions. We have used single-layer MoS_2 as a test material and we expect that this work is a good basis for studies in other monolayer TMDs and in multilayer MoS_2. The electron-phonon interaction also serves to understand the behavior of the resonant Raman spectroscopy. The Eliashberg functions evaluate the exciton-phonon coupling and we can identify the phonon modes to which the excitons couple. We have discovered a different behavior with temperature for the two kinds of excitons existing in MoS_2. First, excitons from the band edges (bound excitons *A* and *B*) are downshifted in energy when temperature increases and the small linewidth does not change significantly. In the case of resonant excitons (*C* exciton), the situation is more complex. Our calculations show that bands far from the band gap have more nonradiative paths available for decaying, as the electron states occupy a wider energy range. Consequently, the nonradiative linewidth is strongly affected by the increase of temperature. The overall result is an optical absorption with a characteristic inhomogeneous broadening, where the *C* peak becomes much broader than the *A* and *B* peaks. Our theoretical spectra agree well with recent experimental measurements. With this contribution, we show the importance of temperature effects, determined by electron-phonon coupling, for a realistic approach to the optical properties of semiconductor 2D materials.

ACKNOWLEDGMENTS

A.M.-S. and L.W. acknowledge support by the National Research Fund, Luxembourg (Projects No. C14/MS/773152/FAST-2DMAT and No. INTER/ANR/13/20/NANOTMD). M.P. acknowledges the support received from the European Science Foundation (ESF) for the activity entitled "Advanced Concepts in *Ab-initio* Simulations of Materials" and from the EC for the RISE Project No. CoExAN GA644076. We acknowledge helpful discussions with M. Calandra about the calculation of electron-phonon matrix elements with spin-orbit coupling. A.M. acknowledges financial support by the Futuro in Ricerca Grant No. RBFR12SW0J of the Italian Ministry of Education, University and Research MIUR, the European Union project MaX Materials design at the eXascale H2020-EINFRA-2015-1, Grant Agreement No. 676598, and Nanoscience Foundries and Fine Analysis - Europe H2020-INFRAIA-2014-2015, Grant Agreement No. 654360.

[1] A. K. Geim and K. S. Novoselov, Nat. Mater. **6**, 183 (2007).
[2] K. Roy, M. Padmanabhan, S. Goswami, T. P. Sai, G. Ramalingam, S. Raghavan, and A. Ghosh, Nat. Nanotechnol. **8**, 826 (2013).
[3] O. Lopez-Sanchez, E. Alarcon Llado, V. Koman, A. Fontcuberta i Morral, A. Radenovic, and A. Kis, ACS Nano **8**, 3042 (2014).
[4] B. Radisavljevic, A. Radenovic, J. Brivio, V. Giacometti, and A. Kis, Nat. Nanotechnol. **6**, 147 (2011).
[5] K. F. Mak, K. L. McGill, J. Park, and P. L. McEuen, Science **344**, 1489 (2014).
[6] X. Hong, J. Kim, S.-F. Shi, Y. Zhang, C. Jin, Y. Sun, S. Tongay, J. Wu, Y. Zhang, and F. Wang, Nat. Nanotechnol. **9**, 682 (2014).
[7] H. Yu, X. Cui, X. Xu, and W. Yao, Natl. Sci. Rev. **2**, 57 (2015).
[8] D. Lembke and A. Kis, ACS Nano **6**, 10070 (2012).
[9] H.-P. Komsa and A. V. Krasheninnikov, Phys. Rev. B **86**, 241201 (2012).
[10] A. Molina-Sánchez, D. Sangalli, K. Hummer, A. Marini, and L. Wirtz, Phys. Rev. B **88**, 045412 (2013).
[11] D. Y. Qiu, F. H. da Jornada, and S. G. Louie, Phys. Rev. Lett. **111**, 216805 (2013).
[12] H.-P. Komsa and A. V. Krasheninnikov, Phys. Rev. B **88**, 085318 (2013).
[13] A. Molina-Sánchez, K. Hummer, and L. Wirtz, Surf. Sci. Rep. **70**, 554 (2015).
[14] D. Wolpert and P. Ampadu, *Temperature Effects in Semiconductors* (Springer, New York, 2012), p. 15.
[15] P. Lautenschlager, P. B. Allen, and M. Cardona, Phys. Rev. B **31**, 2163 (1985).
[16] P. Lautenschlager, M. Garriga, L. Vina, and M. Cardona, Phys. Rev. B **36**, 4821 (1987).
[17] J. A. Miwa, S. Ulstrup, S. G. Sorensen, M. Dendzik, A. G. Cabo, M. Bianchi, J. V. Lauritsen, and P. Hofmann, Phys. Rev. Lett. **114**, 046802 (2015).
[18] M. Cardona, Solid State Commun. **133**, 3 (2005).
[19] F. Giustino, S. G. Louie, and M. L. Cohen, Phys. Rev. Lett. **105**, 265501 (2010).
[20] S. Moser, L. Moreschini, J. Jaćimovic, O. S. Barišić, H. Berger, A. Magrez, Y. J. Chang, K. S. Kim, A. Bostwick, E. Rotenberg, L. Forró, and M. Grioni, Phys. Rev. Lett. **110**, 196403 (2013).

[21] K. Kaasbjerg, K. S. Thygesen, and K. W. Jacobsen, Phys. Rev. B **85**, 115317 (2012).
[22] W. Li, J. Carrete, and N. Mingo, Appl. Phys. Lett. **103**, 253103 (2013).
[23] K. Kaasbjerg, K. S. Bhargavi, and S. S. Kubakaddi, Phys. Rev. B **90**, 165436 (2014).
[24] Y. Ge, W. Wan, W. Feng, D. Xiao, and Y. Yao, Phys. Rev. B **90**, 035414 (2014).
[25] S. Tongay, J. Zhou, C. Ataca, K. Lo, T. S. Matthews, J. Li, J. C. Grossman, and J. Wu, Nano Lett. **12**, 5576 (2012).
[26] Y. Li, A. Chernikov, X. Zhang, A. Rigosi, H. M. Hill, A. M. van der Zande, D. A. Chenet, E.-M. Shih, J. Hone, and T. F. Heinz, Phys. Rev. B **90**, 205422 (2014).
[27] D. W. Latzke, W. Zhang, A. Suslu, T.-R. Chang, H. Lin, H.-T. Jeng, S. Tongay, J. Wu, A. Bansil, and A. Lanzara, Phys. Rev. B **91**, 235202 (2015).
[28] B. R. Carvalho, L. M. Malard, J. M. Alves, C. Fantini, and M. A. Pimenta, Phys. Rev. Lett. **114**, 136403 (2015).
[29] G. Antonius, S. Poncé, P. Boulanger, M. Coté, and X. Gonze, Phys. Rev. Lett. **112**, 215501 (2014).
[30] A. Marini, S. Poncé, and X. Gonze, Phys. Rev. B **91**, 224310 (2015).
[31] A. Marini, Phys. Rev. Lett. **101**, 106405 (2008).
[32] P. Giannozzi, S. Baroni, N. Bonini, M. Calandra, R. Car, C. Cavazzoni, D. Ceresoli, G. L. Chiarotti, M. Cococcioni, I. Dabo, A. D. Corso, S. d. Gironcoli, S. Fabris, G. Fratesi, R. Gebauer, U. Gerstmann, C. Gougoussis, A. Kokalj, M. Lazzeri, L. Martin-Samos, N. Marzari, F. Mauri, R. Mazzarello, S. Paolini, A. Pasquarello, L. Paulatto, C. Sbraccia, S. Scandolo, G. Sclauzero, A. P. Seitsonen, A. Smogunov, P. Umari, and R. M. Wentzcovitch, J. Phys.: Condens. Matter **21**, 395502 (2009).
[33] E. Cannuccia and A. Marini, Phys. Rev. Lett. **107**, 255501 (2011).
[34] C. Verdi and F. Giustino, Phys. Rev. Lett. **115**, 176401 (2015).
[35] A. Marini, C. Hogan, M. Grüning, and D. Varsano, Comput. Phys. Commun. **180**, 1392 (2009).
[36] S. Poncé, Y. Gillet, J. Laflamme Janssen, A. Marini, M. Verstraete, and X. Gonze, J. Chem. Phys. **143**, 102813 (2015).
[37] See Supplemental Material at http://link.aps.org/supplemental/10.1103/PhysRevB.93.155435 for the movie represents the spectral functions from 0 to 1000 K at temperature step of 100 K.
[38] M. B. Stone, I. A. Zaliznyak, T. Hong, C. L. Broholm, and D. H. Reich, Nature (London) **440**, 187 (2006).
[39] X. Li, J. T. Mullen, Z. Jin, K. M. Borysenko, M. Buongiorno Nardelli, and K. W. Kim, Phys. Rev. B **87**, 115418 (2013).
[40] A. Molina-Sánchez and L. Wirtz, Phys. Rev. B **84**, 155413 (2011).
[41] E. Cannuccia and A. Marini, Eur. Phys. J. B **85**, 1 (2012).
[42] B. Monserrat and R. J. Needs, Phys. Rev. B **89**, 214304 (2014).
[43] Y. Gillet, M. Giantomassi, and X. Gonze, Phys. Rev. B **88**, 094305 (2013).
[44] T. Korn, S. Heydrich, M. Hirmer, J. Schmutzler, and C. Schüller, Appl. Phys. Lett. **99**, 102109 (2011).
[45] M. Rohlfing and S. G. Louie, Phys. Rev. B **62**, 4927 (2000).
[46] G. Onida, L. Reining, and A. Rubio, Rev. Mod. Phys. **74**, 601 (2002).
[47] H. Shi, H. Pan, Y.-W. Zhang, and B. I. Yakobson, Phys. Rev. B **87**, 155304 (2013).